Robust characteristics of non-Gaussian fluctuations from the NJL model

Jiunn-Wei Chen, Jian Deng, Hiroaki Kohyama, and Lance Labun

Phys. Rev. D **93**, 034037 — Published 24 February 2016

DOI: 10.1103/PhysRevD.93.034037

Robust characteristics of nongaussian fluctuations from the NJL model

Jiunn-Wei Chen*
Department of Physics and Center for Theoretical Sciences, National Taiwan University, Taipei, 10617 Taiwan
Leung Center for Cosmology and Particle Astrophysics (LeCosPA), National Taiwan University, Taipei, 10617 Taiwan and
Helmholtz-Institut für Strahlen- und Kernphysik and Bethe Center for Theoretical Physics, Universität Bonn, D-53115 Bonn, Germany

Jian Deng†
Key Laboratory of Particle Physics and Particle Irradiation (MOE), School of Physics, Shandong University, Jinan 250100, China

Hiroaki Kohyama‡
Department of Physics and Center for Theoretical Sciences, National Taiwan University, Taipei, 10617 Taiwan

Lance Labun§
Department of Physics, University of Texas, Austin

We evaluate the third- and fourth-order baryon, charge and strangeness susceptibilities near a chiral critical point using the Nambu-Jona-Lasinio model. We identify robust qualitative behaviours of the susceptibilities along hypothetical freeze-out lines that agree with previous model studies. Quantitatively, baryon number fluctuations are the largest in magnitude and thus offer the strongest signal when freeze-out occurs farther away from a critical point. Charge and strangeness susceptibilities also diverge at a critical point, but the area where the divergence dominates is smaller, meaning freeze-out must occur closer to a critical point for a signal to be visible in these observables. In case of strangeness, this is attributable to the relatively large strange quark mass. Plotting the third- and fourth-order susceptibilities against each other along the freeze-out line exhibits clearly their non-montonicity and robust features.

I. INTRODUCTION

Heavy ion collision experiments and lattice simulations are probing the phase diagram of QCD matter to help understand the chiral and deconfinement phase transitions [1]. These experiments have shown that at low density, the transition is a continuous cross-over at $T \sim 165\,\mathrm{MeV}$ [2]. At high density, models lead to the expectation that the transition is first order. This structure would be verified by locating a critical end point in chemical potential–temperature plane where the first order line begins. The heavy ion collision experiments yield statistical observables of QCD matter, including proton number and electric charge fluctuations [3, 4],and lattice studies have developed a variety of approaches to searching for structure at $\mu_B \neq 0$ [5–11].

To interpret the experimental data in terms of the phase diagram, we need to relate them to signatures derived from theory calculations. Since conventional lattice methods are limited to low baryon density by the sign problem, it is useful to complement the investigation with model studies in which we can thoroughly study the phase structure at $\mu \neq 0$. We use the models to identify robust signatures of the critical point, such as consequences of the large correlation length, that would be manifest also near a critical point in QCD. The correlation length becomes large near the critical point (CP) because the CP is a second-order phase transition where the mass term in the Landau effective potential for the order parameter σ vanishes, $m_\sigma \sim \xi^{-1} \to 0$. Therefore, at the CP, the longest wavelength correlations (of order the system "size") can be investigated using the partition function [12]

$$\mathcal{Z} = \int \mathcal{D}\sigma e^{-\frac{1}{T}\int d^3x \Omega[\sigma]} \tag{1}$$

with the Landau effective action

$$\Omega[\sigma] = \Omega_0 + \frac{1}{2}(\vec{\nabla}\sigma)^2 + \frac{m_\sigma^2}{2}\sigma^2 + \frac{\lambda_3}{3}\sigma^3 + \frac{\lambda_4}{4}\sigma^4 + ... \tag{2}$$

Ω_0 is the energy due to the vacuum expectation value (vev) of the order parameter, σ is the fluctuation around this vev, and for fluctuations at wavelengths similar to the system size, we consider only the zero momentum mode, so the kinetic term $(\vec{\nabla}\sigma)^2$ vanishes.

The divergent parts of the fluctuations associated with $\xi \to \infty$ at the CP (an infrared fixed point) are universal for systems within the same universal class. The finite

* jwc@phys.ntu.edu.tw
† jdeng@sdu.edu.cn
‡ kohyama.hiroaki@gmail.com
§ labun@utexas.edu

parts of the fluctuations are model dependent which can be described by higher dimensional operators in the effective action. Using Eq. (1), statistical observables such as baryon number fluctuations are related to fluctuations of the order parameter [12]. For example, higher order, non-Gaussian fluctuation moments are more sensitive to a critical point because they diverge with a larger power of the correlation length, as shown for the third and fourth order susceptibilities [13–15].

In this approach, we hypothesize the presence of a critical point, investigate the consequences, and compare them to data. It is important to bear in mind that the conditions we identify for a critical point can only be necessary conditions but not sufficient conditions. Also, there are many assumptions in our attempt to compare with heavy ion data. For example, we assume the fireball is near thermal equilibrium at freeze-out, though critical slowing of dynamics would be important if the fireball approaches the critical point chemical potential and temperature [16]. Additionally, there can be changes in expansion dynamics and interactions that produce variations in particle spectra and acceptance independent of critical phenomena, whose fluctuations must also be controlled for [17]. To claim evidence of a critical point in this context, we should identify as many model-independent signatures as possible to corroborate interpretation of the data in terms of a critical point.

In this work, we study the Nambu-Jona-Lasinio (NJL) model, which is a QCD inspired field theoretic model with spontaneous breaking of Chiral symmetry [18–20]. The model comprises distinct flavors of quarks that interact via (effective) point-like 4-fermion operators. At low density and temperature, the model exhibits a non-zero chiral condensate $\langle\bar{\psi}\psi\rangle \neq 0$ [21–25]. The goal is to identify, in the NJL model results, characteristics of fluctuation observables that are predicted to be model-independent by analysis such as given in [13, 15]. Previous work using the NJL model has focused on third moments [14], or electric charge susceptibilities [26]. Numerical studies of the susceptibilities have also used the Polyakov-loop improved NJL model (PNJL) [27] and Dyson-Schwinger approaches [28]. As the Polyakov-loop does not introduce any new effective degrees of freedom at the chiral critical point, the PNJL model is in the same (Ising) universality class as the NJL model and QCD. Therefore, the NJL suffices as a first step to investigate robust and model-independent fluctuation signatures of the chiral critical point. Although an interesting next step to check the conclusions of this paper in the PNJL model, we expect our results to be reproduced. Indeed, model-independent characteristics we discuss below have been confirmed and cross-checked in the Ising [15] and Gross-Neveu (GN) models [29].

There are two main goals in this work. The first goal is to make use of the flavor dependence in the NJL model to compute the complete set of susceptibilities on the phase diagram. The currently open-ended experimental search motivates a thorough and systematic search of the possible experimental observables to check all candidate measurements that can aid the identification of the CEP. The second goal is to check whether some model-independent features obtained from a general effective potential analysis then confirmed by the GN model [29] will remain in the NJL model, which belongs to the same universality class with QCD at the CP. These features include: (1) The negative σ-kurtosis ($\langle\sigma^4\rangle - 3\langle\sigma^2\rangle^2 < 0$) region occurs almost entirely in the symmetric (normal) phase. (2) However, in addition to the σ-kurtosis, there are more critical-mode correlators contributing to the fourth-order baryon number susceptibility ($\partial^4 \ln Z/\partial\mu_B^4$) to determine its negative region. (3) The peaks in non-Gaussian susceptibilities on a freeze out line obey an ordering in temperature.

Among these features, we expect the first to be robust, because the σ fluctuations can be understood from the shape of the effective potential around the critical point [29]. We also expect the second to happen, that is, there are other terms as important as the σ-kurtosis to determine the negative region of ($\partial^4 \ln Z/\partial\mu_B^4$), again due to analysis of a general effective action in Ref. [29] to identify terms with leading power divergence in ξ near the CP. We will check it numerically using the NJL model. We will also show the third feature occurs in the NJL, supporting its robustness as an observable feature of critical fluctuations.

II. COMPLETE SET OF FLUCTUATION OBSERVABLES

Fluctuations in conserved charges are important observables because they can be obtained in principle from HIC experiments as well as lattice simulations. Not all fluctuation moments can be measured in practice, and we will discuss below the observationally most relevant subset. The fluctuation moments are derivatives of the partition function with respect to the chemical potentials of the conserved charges:

$$\chi_{\alpha\beta} = \frac{\partial^2 \ln \mathcal{Z}}{\partial\mu_\alpha \partial\mu_\beta}, \quad \chi_{\alpha\beta\gamma} = \frac{\partial^3 \ln \mathcal{Z}}{\partial\mu_\alpha \partial\mu_\beta \partial\mu_\gamma}, ... \qquad (3)$$

If $\alpha = \beta = ...$ we shall also use $\chi_\alpha^{(n)} = \partial^n \ln \mathcal{Z}/\partial\mu_\alpha^n$. Recall the first derivative is the expected number, $\partial \ln \mathcal{Z}/\partial\mu_X \equiv \langle N_X\rangle$, which is conserved and therefore constrained by the initial conditions. For example, since protons and neutrons comprise only up and down quarks and strangeness is conserved by QCD reactions, $\langle N_s\rangle = 0$. On the other hand, since the heavy nuclei typically contain more neutrons than protons, the initial state has an isospin asymmetry.

At quark level, we have three independent chemical potentials μ_u, μ_d, and μ_s associated with the conserved quark numbers for u, d, and s quarks, respectively. To compare to experiment, we use the basis of conserved charges $\{B, Q, S\}$. The hadron-level strangeness (large

S) is defined so that K^+ has $S = +1$ in agreement with the experimental notation and opposite the quark-level definition of the strange charge (small s) where the strange quark has $s = -1$ and antistrange quark has $s = +1$. We will use the $\{q, I, s\}$ basis of charges, where $2\mu_q = \mu_u + \mu_d$ and $\mu_I = \mu_u - \mu_d$. Since the isospin potential μ_I is also measurable at hadron-level, we can use observations to constrain the chemical potentials, and so also the set of susceptibilities we need to evaluate.

The chemical potentials $\mu_B, \mu_Q, \mu_S, \mu_I$ at chemical freeze-out are determined by fitting the observed particles yields to a statistical model of hadronization in the fireball. Limited acceptance and experimental effects can mean the fit values of the chemical potentials differ from the theoretical expectation. The inital conditions for two Au nuclei imply that $\langle Q\rangle/\langle B\rangle \simeq 0.4$ if all nucleons participate in the collision, but in general the ratio is centrality dependent and varies from event to event. Fixing the ratio to 0.4 would imply that μ_I varies with μ_B but always remains in the range $-10 < \mu_I < 0$ MeV ($\mu_I = 0$ yields $\langle Q\rangle/\langle B\rangle = 0.5$, which is close to 0.4 already). For such small $|\mu_I|$ the change in the phase diagram is small (corrections of order $(\mu_I/\mu_{Bc})^2$ or $(\mu_I/T_c)^2$ near the CP), and we have checked that the corresponding impact on the observables is not noticeable. To fix μ_s, the data indicate that when collision energy per nucleon pair in the center-of-mass frame ($\sqrt{s_{NN}}$) is 7.7, 39, 200 GeV, $\mu_B/3$ is ∼130, 30, 10 GeV and μ_S is ∼90, 20, 5, respectively [30]. Using Eq. (8) and isospin symmetry $\mu_u \simeq \mu_d$, this implies μ_s is ∼40, 10, 5 GeV, even though theoretically $\langle N_s\rangle = 0$ in the initial state. However, given $\mu_s \lesssim 40$ MeV which is smaller than the lower range on the strange quark (current) mass $m_s \gtrsim 90$ MeV, it is a good approximation to set $\mu_s = 0$ in our model calculations: dependence of the phase diagram on μ_s is weak as long as for $\mu_s \leq m_s$.

It is worth noting here that one piece of evidence for non-equilibrium at chemical freeze-out is that particle yield fits are improved by including a strange quark quenching factor γ_s, which observationally is ≤ 1. This smaller-than-equilibrium abundance of both s and $\bar{s}$ can be understood considering that the phase space for producing $s, \bar{s}$ quarks is smaller due to their moderately large mass $m_s \gtrsim 90$ MeV compared to the temperature $T \lesssim 160$ MeV. That is, a substantially smaller fraction of gluons (or $q\bar{q}$ pairs) collide with center-of-mass energy $\geq 2m_s > 180$ MeV, which suppresses the reaction rate for production in comparison to the lifetime of the fireball [31]. Although it impacts the absolute abundance of measured strange particles, it is linearly independent of μ_s that controls net strangeness, i.e. the number of strange minus the number of antistrange quarks $N_s - N_{\bar{s}}$. With $\mu_s = 0$, there is no violation of strange quark number independent the value of γ_s.

Additionally, up-to-date analysis of the charged pion ratio $N(\pi^-)/N(\pi^+) \simeq e^{2\mu_Q/T}$ has consistently concluded that $\mu_Q = \mu_I = 0$ for all $\sqrt{s_{NN}} \geq 7.7$ GeV. However, the μ_Q fit is generally dependent on the fit temperature and centrality, and some variation as a function of $\sqrt{s_{NN}}$ is expected seeing as the total particle multiplicity is much higher for larger $\sqrt{s_{NN}}$. Even having small, nonzero μ_Q would not change our results however, because the phase diagram is weakly dependent on μ_Q as long as $\mu_Q = \mu_I \ll m_\pi/2 \simeq 65$ MeV (this is also found in [33]). Therefore, in our work we shall for simplicity set $\mu_I = 0$ for all μ_B.

With $\mu_s = \mu_I = 0$, a complete set of nontrivial susceptibilities up to fourth order is:

$$\begin{aligned}&\chi_{qq}, \chi_{II}, \chi_{ss},\\ &\chi_q^{(3)}, \chi_{qss}, \chi_{qII},\\ &\chi_q^{(4)}, \chi_{qqII}, \chi_{qqss}, \chi_I^{(4)}, \chi_{IIss}, \chi_s^{(4)}\end{aligned}$$

These are easy to count in the $\{q, I, s\}$ basis, because $\mu_I = \mu_s = 0$ implies that odd-order derivatives of μ_I vanish identically. When we choose another basis, there can only be 3, 3, and 6 independent susceptibilities at 2nd, 3rd and 4th order respectively. These are plotted in Figs. 2, 3, 5 and 6.

While the long-wavelength correlations are dominated by the iso-scalar critical mode σ and the isospin chemical potential is "small" (as defined below) this relation shows that charge fluctuations diverge like the baryon fluctuations near the critical point [34]. As explained in the next section and Appendix B, the second-order isospin and strange susceptibilities do not have a singularity at the critical point, even in the presence of flavor mixing. By direct computation of χ_Q and χ_B in the NJL model below, we will verify this fact. On the other hand, because the correlation length in the fireball may peak at ~ 3 fm, only about twice the thermal correlation length (and much smaller than infinity), the difference between the singular iso-scalar critical mode contribution and the smooth model-dependent contributions to correlations may be less dramatic.

To relate the B, Q, S susceptibilities to the derivatives with respect to quark susceptibilities we need to rewrite partition function in terms of the B, Q, S charges. The grand canonical partition function can be expressed as

$$\mathcal{Z} = \mathrm{Tr} e^{-\beta(\hat{H} - \mu_X \hat{N}_X)} \tag{4}$$

where $\hat{N}_X$ is the number operator, i.e. the time component of the conserved current. This implies that the quark chemical potentials μ_q, μ_I, μ_s are related to the chemical potentials associated with observable numbers μ_B, μ_Q, μ_S using the linear relations between the particle numbers. Starting from the definitions

$$N_q \equiv N_u + N_d, \quad N_I \equiv \frac{1}{2}(N_u - N_d)\,,$$

we have

$$N_B = \frac{1}{3}(N_q + N_s) = \frac{1}{3}(N_u + N_d + N_s) \tag{5}$$

$$N_Q = \frac{1}{6}N_q + N_I - \frac{1}{3}N_s = \frac{1}{3}(2N_u - N_d - N_s) \tag{6}$$

$$N_S = -N_s \tag{7}$$

These relations lead to

$$\mu_B = 3\mu_q - \frac{1}{2}\mu_I \tag{8a}$$

$$\mu_Q = \mu_I \tag{8b}$$

$$\mu_S = \mu_q - \frac{1}{2}\mu_I - \mu_s \tag{8c}$$

and conversely

$$\mu_q = \frac{1}{3}\mu_B + \frac{1}{6}\mu_Q \tag{9a}$$

$$\mu_I = \mu_Q \tag{9b}$$

$$\mu_s = \frac{1}{3}\mu_B - \frac{1}{3}\mu_Q - \mu_S \tag{9c}$$

Using Eq. (9) we can rewrite the observable susceptibilities in terms of quark susceptibilities, which are derivatives of the NJL potential. For example, the baryon susceptibility is

$$\begin{aligned}\chi_B =& \frac{\partial^2 \ln \mathcal{Z}}{\partial \mu_B^2} = \left(\frac{1}{3}\frac{\partial}{\partial \mu_q} + \frac{1}{3}\frac{\partial}{\partial \mu_s}\right)^2 \ln \mathcal{Z} \\ =& \frac{1}{9}\chi_{qq} + \frac{2}{9}\chi_{qs} + \frac{1}{9}\chi_{ss}\end{aligned} \tag{10}$$

Since net strangeness is conserved and equal to zero $\langle N_s \rangle = 0$ independent of the u, d chemical potentials,

$$\chi_{qs} = \frac{\partial}{\partial \mu_q}\langle N_s \rangle = 0 \tag{11}$$

so that the second term in Eq. (10) vanishes. Finally, we have

$$\chi_B = \frac{1}{9}\chi_{qq} + \frac{1}{9}\chi_{ss} \tag{12}$$

Similarly, the charge susceptibility simplifies

$$\chi_Q = \frac{1}{36}\chi_{qq} + \chi_{II} + \frac{1}{9}\chi_{ss} \tag{13}$$

because the cross term $\propto \chi_{us}$ is zero. Note the presence of the strange susceptibility. This shows that both the charge and baryon fluctuations are dominated by the light quark fluctuations, as we expect [34]. The strangehadron susceptibility is

$$\chi_S = \chi_s \tag{14}$$

III. SUSCEPTIBILITIES WITH FLAVOR

In Ref. [29], the explicit expressions for the quark (baryon) susceptibilities $\chi_B^{(3)}, \chi_B^{(4)}$ in terms of autocorrelation functions of the σ zero mode $\langle \sigma^n \rangle$ were derived for the GN model. The k-th order susceptibility requires only correlation functions of k-th order and lower, see Eqs. (6), (7), and (8) in [29]. While higher order susceptibilities typically diverge with larger powers of the correlation length ξ [13], we found that the corresponding autocorrelation function $\langle \sigma^n \rangle$ does *not* always provide the complete leading order contribution to χ_n. It also implies that the evaluation of χ_n can be organized diagrammatically corresponding to a finite set of terms in perturbation theory. As we extend the analysis to NJL, the diagrammatic expansion becomes more complicated, however, we can use it to help explain the behaviour of strange quark susceptibilities near the critical point.

When writing these susceptibilities in terms of order parameter fluctuations, we must include three condensates, one for each flavor, and hence three fluctuation fields σ_α, $\alpha = u, d, s$. Due to the anomaly-induced six-quark interaction vertex, the σ "correlator" (statistical covariance) $\partial^2\Omega/\partial\sigma_\alpha\partial\sigma_\beta$ is not diagonal in flavor. This fact is derived and a brief description of the diagrammatic system is found in Appendix B.

We have checked numerically that the expansion in terms of σ correlators is equivalent to taking the μ derivatives directly at the minimum of the effective potential by brute force, e.g. a finite difference method. The σ-correlator diagrams provide an easier method to organize and analyze the many terms arising from the evaluation of higher order and multi-flavor susceptibilities.

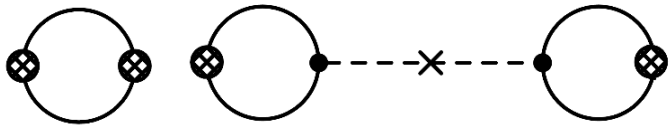

FIG. 1. Diagrams (a) and (b) respectively correspond to the first and second terms in Eq. (B3). Each crossed circle denotes an insertion of the $\bar{q}_\alpha q_\alpha$ operator arising from taking a μ_α derivative to the pressure which is proportional to the logarithm of the partition function. The solid and dashed lines denote the quark and the σ_α propagators. The cross denotes the flavor mixing of the σ propagators.

Using the diagrammatic system developed in Appendix B, we can quickly identify large contributions to flavor-dependent observables. As mentioned above, the critical mode is associated with light quarks, since this transition occurs at smaller μ_B. Therefore the most divergent contributions are n-point correlation functions of the σ_q fluctuations.

The diagrams shown in Figure 1 explain the behaviour of the second order susceptibilities χ_{II} and χ_{ss}. Since the first derivatives with respect to μ_I and μ_s vanish identically at $\mu_I, \mu_s = 0$, the diagram on the right vanishes because it has only a single μ-derivative acting on the distribution function. As a result, there are no contributions involving σ-correlators to these susceptibilities, and they show no divergence.

In Figures 2, 3, 5 and 6 we display the complete set of quark susceptibilities $\chi_{\alpha\beta\ldots}$ up to the fourth deriva-

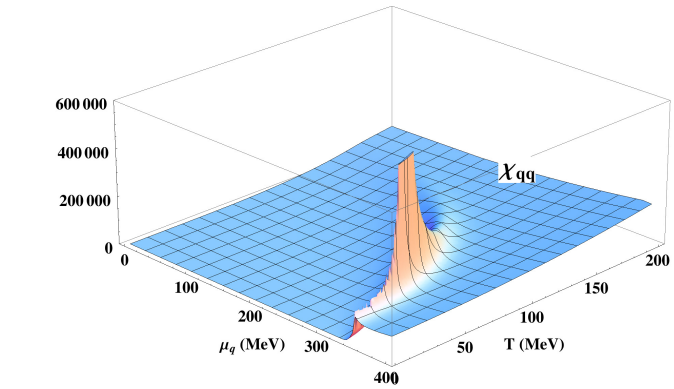

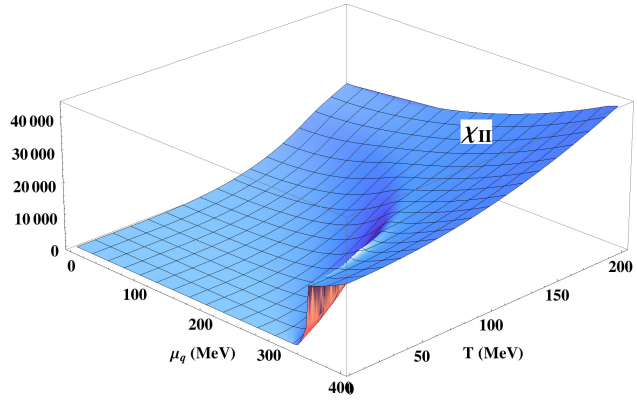

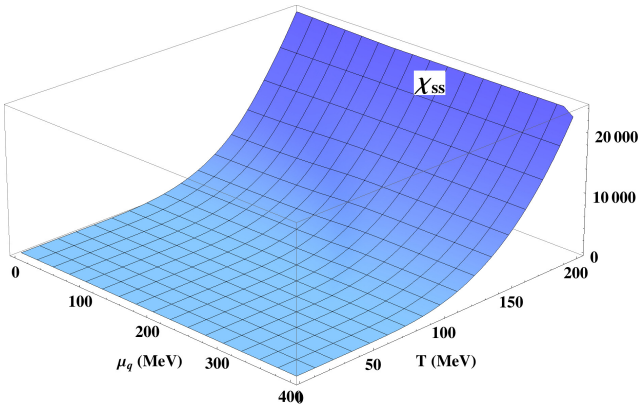

FIG. 2. The quark χ_{qq}, isospin χ_{II}, and strange(-quark) χ_{ss} susceptibilities. There is no singularity at the CEP in χ_{II} or χ_{ss} as expected, considering no σ-correlator terms contribute.

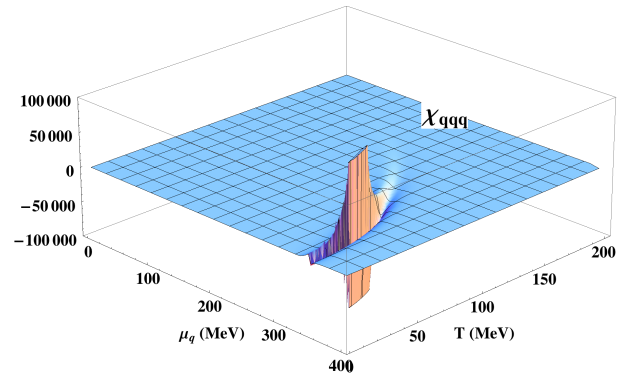

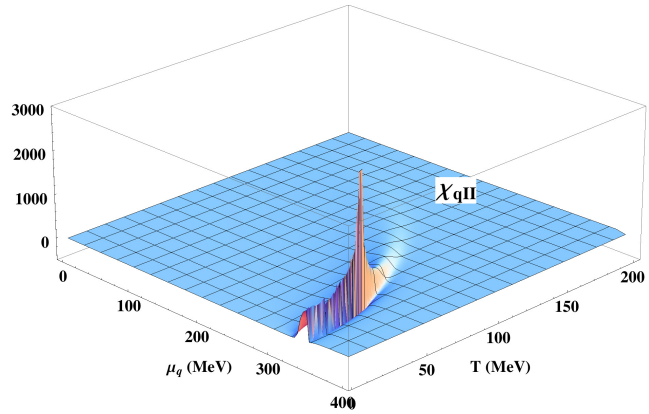

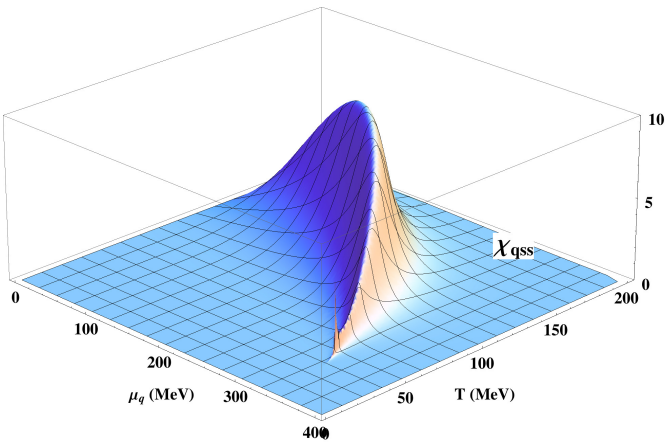

FIG. 3. The non-vanishing third order susceptibilities $\chi_{qqq}, \chi_{qII}, \chi_{qss}$ can be checked by taking the μ_q derivative of the second order susceptibilities in Fig. 2. Note the scale of the vertical axis here: the variation in χ_{ss} implied by its derivative is barely visible in Fig. 2 and is confirmed by plotting constant T lines. χ_{qII} and χ_{qss} have singularities due to the new contributing diagram in Fig. 4.

tives, from which we need to construct the fluctuations of observables. We consider this an important intermediate step to have on record, to verify the analytic arguments which susceptibilities are singular and for the purposes of comparison to broad experimental searches, which may also consider other susceptibilities. We plot the susceptibilities on the phase diagram with respect to quark chemical potential, which is linearly related to the observable baryon susceptibility $\mu_B = 3\mu_q$ Eq. (9) seeing that we consider the case $\mu_I = 0$. (This differs from the definition of μ_B in [35]).

The third order susceptibilities are straightforwardly understood since each is a single μ_q derivative on a second order susceptibilities. Thus, we can confirm by eye the correct behaviours: χ_{qqq} is odd across the first order line, corresponding to the peak seen in χ_{qq}. χ_{qII} has a peak around the first-order line, corresponding to the jump in χ_{II} but remains positive at high μ since χ_{II} continues with positive derivative. The variation of χ_{ss}, exhibited

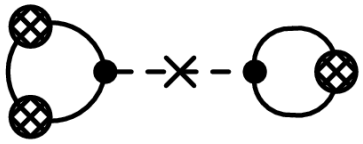

FIG. 4. Diagram contributing the singularity to χ_{qII} and χ_{qss}.

by nonzero χ_{qss}, is too small in magnitude to see in Fig. 2. The derivative with μ_q contributes a singularity at the CEP to each χ_{qII} and χ_{qss}, which arises from a new nonzero diagram, shown in Fig. 4.

Among the fourth order susceptibilities, three $\chi_q^{(4)}, \chi_{qqII}, \chi_{qqss}$ can be understood in the same way as the third order susceptibilities looking at the μ_q-derivatives of the previous plots. For the other three, we can use the diagrammatic analysis.

$\chi_s^{(4)}$ can have a singular contribution. Again, the diagrams contributing are severely constrained by the fact that odd derivatives in μ_s vanish. The only two diagrams with an even of number of μ_s derivatives on the external legs are shown in Figure 7. The diagram on the right does contain a σ correlator, which is flavor-diagonal, connecting one s distribution function (loop) to a second. This correlator is also singular at the light quark critical point, due to the flavor coupling term in the NJL Lagrangian. This fact is recognized in many studies of NJL [27], that the strange condensate also has a small discontinuity across the first order line. However, the singularity at the CEP is suppressed quantitatively by the small discontinuity and large strange quark bare mass. With high precision numerics, it becomes visible in Figure 10 below.

The same diagrams in Fig. 7 contribute to $\chi_I^{(4)}$. With the presence of σ-correlators for the light quarks, we can expect some singularity, larger than in $\chi_s^{(4)}$ but smaller than in $\chi_q^{(4)}$ due to some cancellation of leading terms. For χ_{IIss} only the diagram on the right in Fig. 7 contributes (because the $(\bar{q}_I q_I)^2 (\bar{q}_s q_s)^2$ operators cannot be contracted to a single loop). The σ-correlator implies χ_{IIss} is singular, but again the divergence is relevant only in a very small region, even accounting for the ξ-scaling of the coefficients weighting each σ-correlator contribution.

The cross-correlation in flavor χ_{qqss} receives a larger singular contribution. To see this, consider the four possible diagrams shown in Figure 8. In each diagram, there are at least two σ_q propagators, which together give a factor $\propto \xi^4$. Further, we can estimate that the dominant effect near the CEP is the diagram with the σ_u 3-point function: involving 3 σ correlators (each scaling as ξ^2) and the 3-point vertex (scaling as $(\xi T)^{-1.5}$, obtained by solving the gap equation near the CP), the diagrams has an overall scaling $\sim \xi^{4.5}$, before the ξ-dependence of the coefficient is applied. The dominance of this term is confirmed numerically. However, the overall magnitude of the peak is exponentially suppressed by the strange mass as compared to the singularities in light quark susceptibilities, which we have checked by varying the bare mass of strange quark.

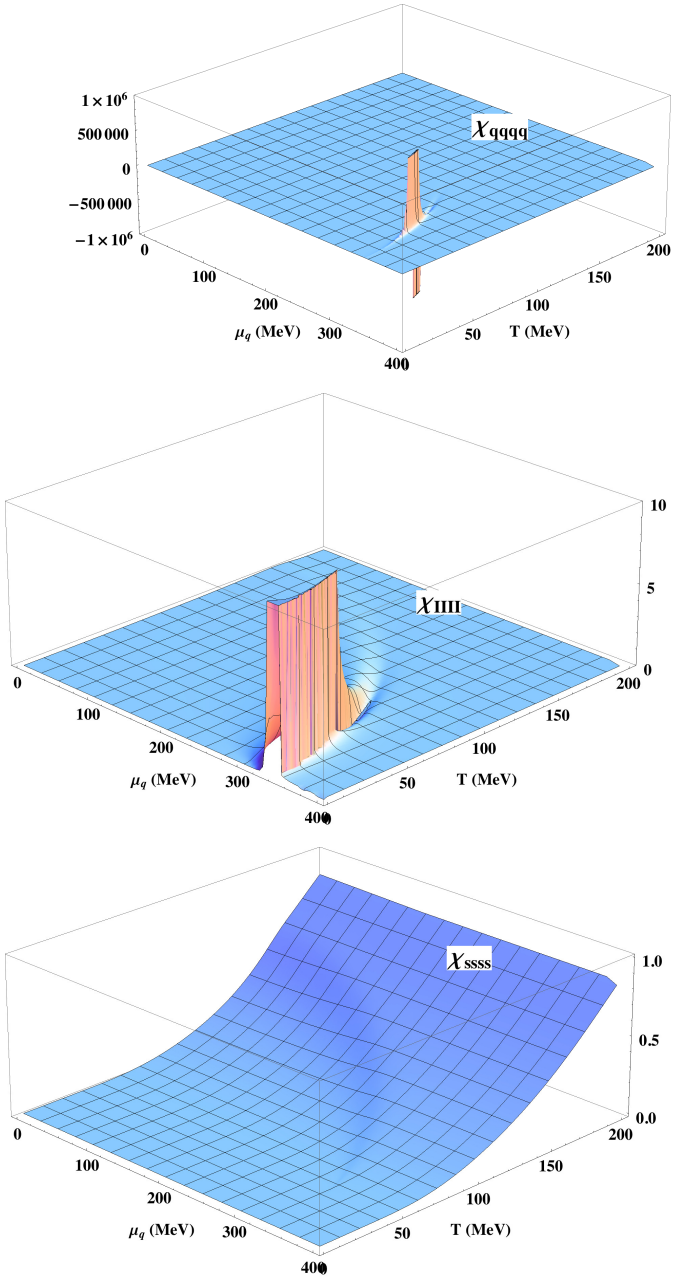

FIG. 5. The fourth-order susceptibilities, $\chi_q^{(4)}$, $\chi_I^{(4)}$ and $\chi_s^{(4)}$. Both $\chi_I^{(4)}$ and $\chi_s^{(4)}$ have singularities at the CEP, due to the diagram in Fig. 7. However, the relative magnitude of the peaks in $\chi_q^{(4)}$ and $\chi_I^{(4)}$ means that $\chi_q^{(4)}$ still dominates the charge susceptibility $\chi_Q^{(4)}$ despite the small coefficient seen in Eq. (16). The singularity in $\chi_s^{(4)}$ is seen in $m_2(S)$ defined in Eq. (17) and plotted (Fig. 10) below.

Writing out the nongaussian hadron-level susceptibil-

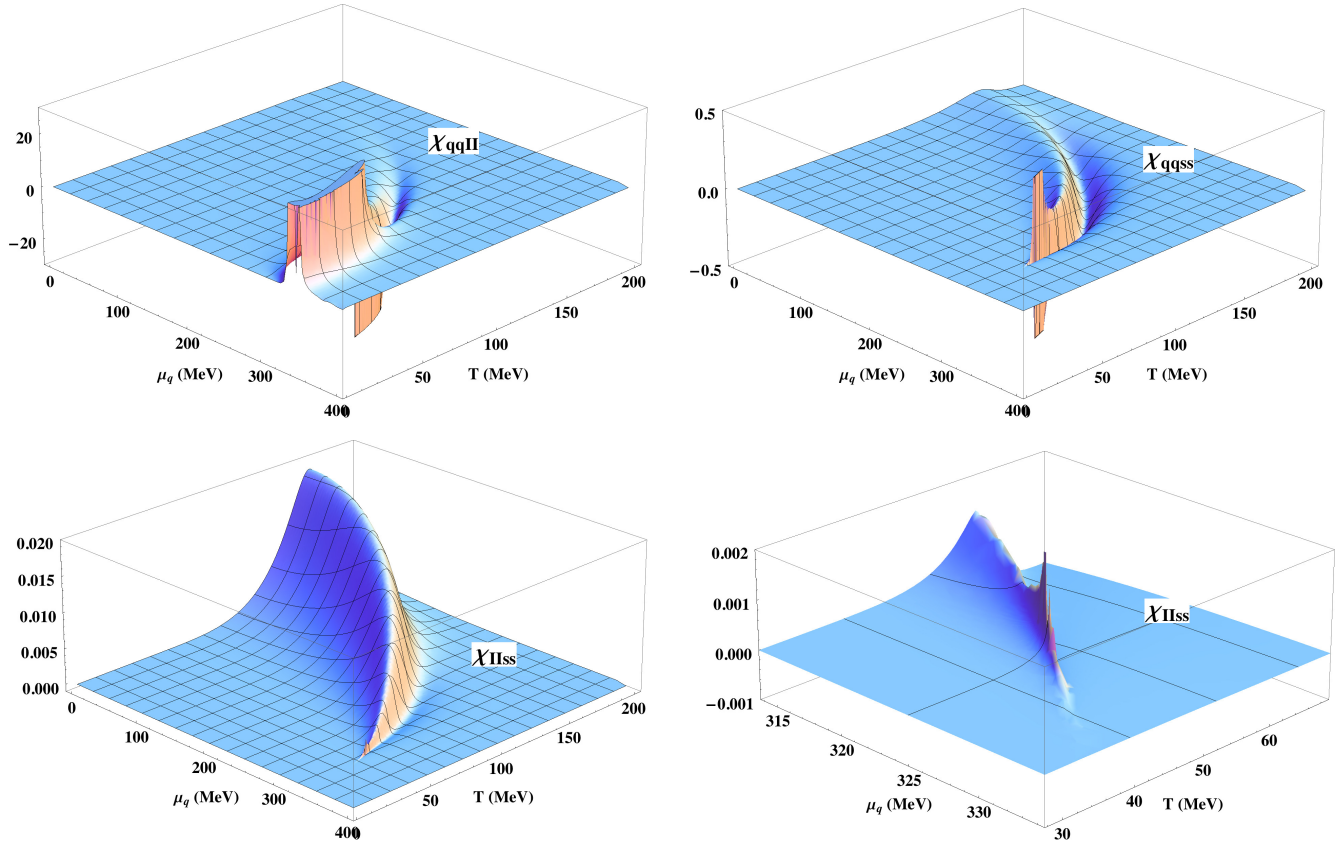

FIG. 6. The fourth-order susceptibilities, χ_{qqII}, χ_{qqss} and χ_{IIss}. χ_{qqII} and χ_{qqss} receive contributions from several singular diagrams, shown in Fig. 8, but the overall magnitude remains small, suppressed by the strange quark mass in the case of χ_{qqss}. χ_{IIss} also has a singularity from the same diagram shown in Fig. 7.

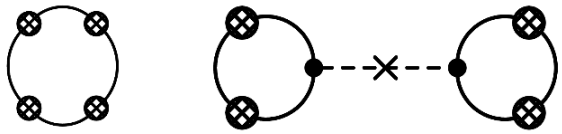

FIG. 7. Diagrams in the expansion of $\chi_s^{(4)}$ and $\chi_I^{(4)}$. Due to the $\mu \leftrightarrow -\mu$ symmetry around $\mu = 0$, the only nonvanishing diagram involving a σ field correlator is at right, and can only involve the σ_s (or σ_I) order parameter field.

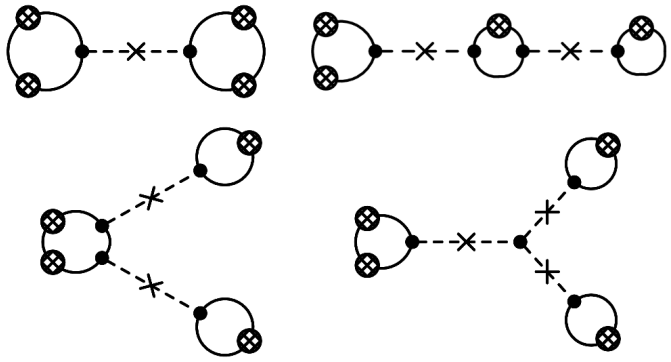

FIG. 8. Diagrams in the expansion of χ_{uuss}

ities, as expected, only 3 third-order susceptibilities and 6 fourth-order susceptibilities are linearly independent.

The third order susceptibilities are

$$\chi_B^{(3)} = \frac{1}{27}\chi_q^{(3)} + \frac{1}{9}\chi_{qss} \tag{15a}$$
$$\chi_Q^{(3)} = \frac{1}{216}\chi_q^{(3)} + \frac{1}{2}\chi_{qII} + \frac{1}{18}\chi_{qss} \tag{15b}$$
$$\chi_S^{(3)} = 0 \tag{15c}$$
$$\chi_{BBQ} = \frac{1}{54}\chi_q^{(3)} - \frac{1}{18}\chi_{qss} \tag{15d}$$
$$\chi_{BBS} = -\frac{2}{9}\chi_{qss} \tag{15e}$$
$$\chi_{BQQ} = \frac{1}{108}\chi_{qqq} + \frac{1}{3}\chi_{qII} \tag{15f}$$
$$\frac{1}{6}\chi_{BSS} = \chi_{BQS} = \frac{1}{3}\chi_{QSS} = \frac{1}{2}\chi_{QSS} = \frac{1}{18}\chi_{qss} \tag{15g}$$

and the fourth order susceptibilities are

$$\chi_B^{(4)} = \frac{1}{81}\chi_q^{(4)} + \frac{2}{27}\chi_{qqss} + \frac{1}{81}\chi_s^{(4)} \tag{16a}$$
$$\chi_Q^{(4)} = \frac{1}{1296}\chi_q^{(4)} + \frac{1}{54}\chi_{qqss} + \frac{1}{6}\chi_{qqII} + \chi_I^{(4)} + \frac{2}{3}\chi_{IIss} + \frac{1}{81}\chi_s^{(4)} \tag{16b}$$
$$\chi_S^{(4)} = \chi_s^{(4)} \tag{16c}$$
$$\chi_{BBBQ} = \frac{1}{162}\chi_q^{(4)} - \frac{1}{54}\chi_{qqss} - \frac{1}{81}\chi_s^{(4)} \tag{16d}$$
$$\chi_{BBBS} = -\frac{1}{9}\chi_{qqss} - \frac{1}{27}\chi_s^{(4)} \tag{16e}$$
$$\chi_{BBQQ} = \frac{1}{324}\chi_q^{(4)} - \frac{1}{108}\chi_{qqss} + \frac{1}{9}\chi_{qqII} + \frac{1}{9}\chi_{IIss} + \frac{1}{81}\chi_s^{(4)} \tag{16f}$$
$$\chi_{BBSS} = \frac{1}{9}\chi_{qqss} + \frac{1}{9}\chi_s^{(4)} \tag{16g}$$
$$\chi_{BQQQ} = \frac{1}{648}\chi_q^{(4)} + \frac{1}{108}\chi_{qqss} + \frac{1}{6}\chi_{qqII} - \frac{1}{3}\chi_{IIss} - \frac{1}{81}\chi_s^{(4)} \tag{16h}$$
$$\chi_{BQQS} = \frac{1}{36}\chi_{qqss} - \frac{1}{3}\chi_{IIss} - \frac{1}{27}\chi_s^{(4)} \tag{16i}$$
$$\chi_{BQSS} = \frac{1}{18}\chi_{qqss} - \frac{1}{9}\chi_s^{(4)} \tag{16j}$$
$$\chi_{QQQS} = \frac{1}{36}\chi_{qqss} + \chi_{IIss} + \frac{1}{27}\chi_s^{(4)} \tag{16k}$$
$$\chi_{QQSS} = \frac{1}{36}\chi_{qqss} + \chi_{IIss} + \frac{1}{9}\chi_s^{(4)} \tag{16l}$$
$$\chi_{BBQS} = -\frac{1}{9}\chi_{BSSS} = \frac{1}{9}\chi_{QSSS} = \frac{1}{27}\chi_s^{(4)} \tag{16m}$$

Based on the above analysis, the behaviour of these susceptibilities near a critical point (magnitude and shape) are dominated by the light quark susceptibilities, such as $\chi_q^{(3)}$ at third order and $\chi_q^{(4)}$ at fourth order. Only in observables without these two terms can the singularity due to the strange quark fluctuations be visible. We will see these effects in the following section.

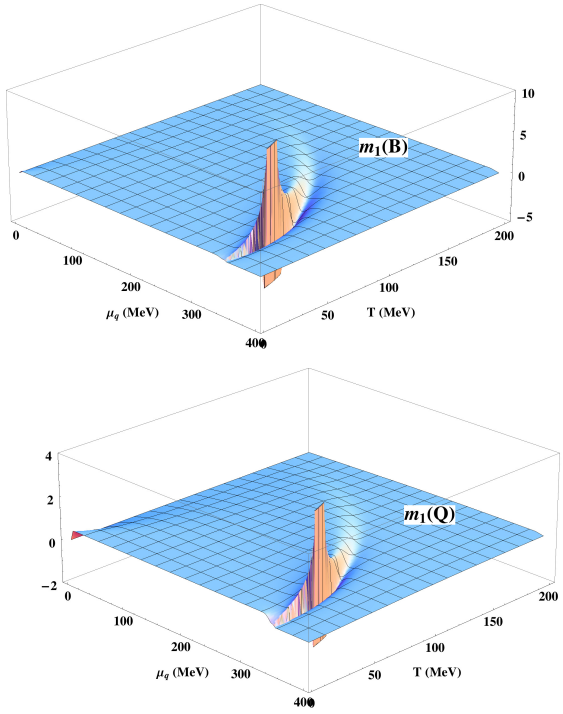

FIG. 9. m_1 for B, Q on the phase diagram. With $\mu_s = 0$, m_1 for S is zero for all μ_q, T.

IV. CHARACTERISTICS OF THE SUSCEPTIBILITIES

Here we display the numerical results for the fluctuation observables of primary interest. The volume factors in the susceptibilities are removed by considering ratios

$$m_1(X) = \frac{T\chi_X^{(3)}}{\chi_{XX}}, \qquad m_2(X) = \frac{T^2\chi_X^{(4)}}{\chi_{XX}}, \tag{17}$$

for $X = B, Q, S$. We display the results for m_1, m_2 for each conserved charge in Figures 9 and 10. Note that $m_1(S) \propto \chi_{sss} = 0$, so we do not show it.

In $m_2(S)$, we see the divergence in $\chi_s^{(4)}$ explained above. However, as seen in the scaling of the axes, the magnitude of the singularity and area of the critical region are small. It requires high numerical precision to make the effect visible. Similarly we can form observable ratios from other third- and fourth-order hadron-level susceptibilities, involving strangeness or cross-correlations in baryon and charge fluctuations. The ratio $T\chi_{BSS}/\chi_{BB}$ is proportional to χ_{qss}; however, the divergence in χ_{qss} is effectively canceled by the divergence in χ_{qq}, as suggested by comparing Fig.4 and Fig.1. Consequently, the ratio shows no singular behaviour at the CEP. For the ratio $T^2\chi_{BBSS}/\chi_{BB}$, χ_{uuss} in the numerator diverges with a larger power of ξ than the denominator, as seen by comparing the diagrams in Fig.8 and Fig.1, so there is a visible singularity peak at CEP. The shape of $T^2\chi_{BBQQ}/\chi_{BB}$ is very similar to $m_2(B)$

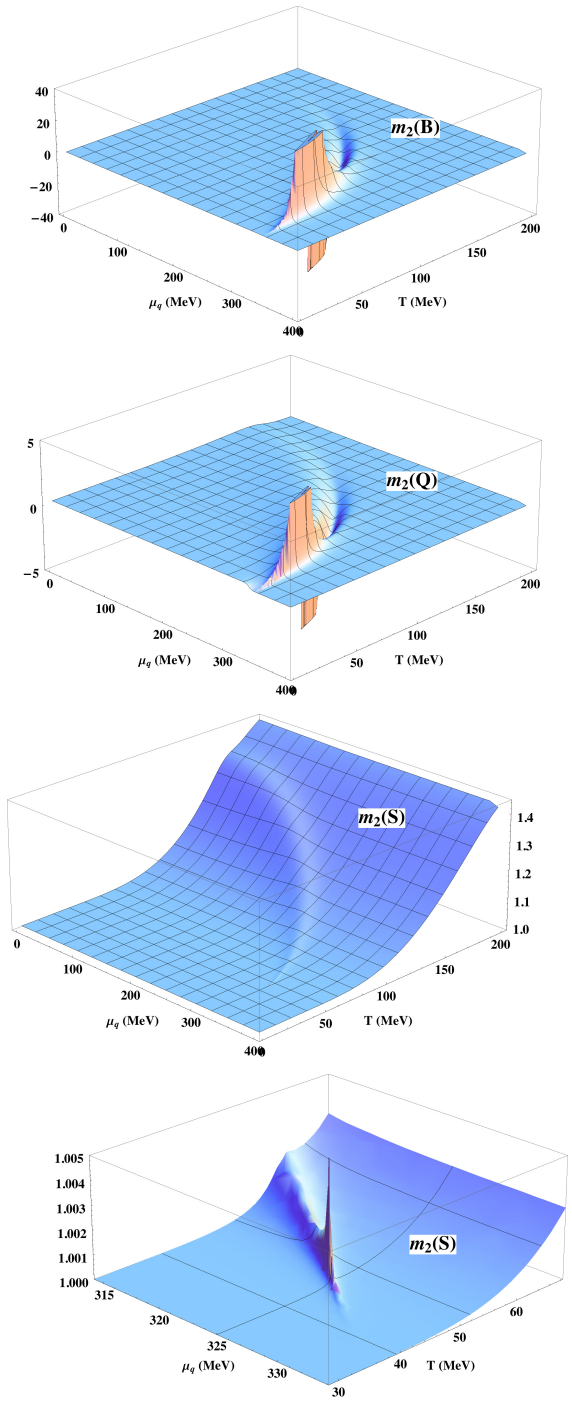

FIG. 10. m_2 for each of B, Q, S on the phase diagram. The bottom figure exhibits the singularity in $\chi_S^{(4)} = \chi_s^{(4)}$ coming from the diagram Fig. 7.

and $m_2(Q)$, because all three are dominated by the light quark susceptibilities. The results in Fig. 11 confirm that singularities in the isospin and strangeness susceptibilities make small impact on the observable fluctuations.

The area of the positive and negative regions in the m_1, m_2 for B, Q are seen more clearly in the density plots Figs. 12 and 13. The shapes are consistent with previous results [14]. Note the area of the critical region for the baryon number fluctuations is larger than the same region for charge fluctuations, consistent with the overall larger magnitude of the baryon fluctuations seen in Figs. 9 and 10. The area of the critical region for strangeness is smaller still than for the charge fluctuations, and is due to the small effect of the singularity on the strange quark susceptibilities away from the critical point. In the context of the conventional equilibrium fluctuations framework to look for signatures of a critical point, the large mass of the strange quark (comparable to T, μ_q) suppresses fluctuation observables. However, this analysis does not account for the possible impact of nonequilibrium dynamics, such as critical slowing, on strangeness yields and fluctuations.

In addition, following [15] and [29], we show the result of extracting the values of m_1 and m_2 along various hypothetical freeze-out lines chosen to pass varying distances from the critical point. The freeze-out lines are shown in the top frame of Fig. 14. The behaviour of $m_1(B)$ and $m_2(B)$ along the freeze-out lines shows good qualitative agreement with the previous GN model calculations, supporting the robustness of these shapes and their variation with distance from the CEP. The profile of charge fluctuations along the freeze-out line is very similar to the baryon fluctuations, with the apparent difference due to the overall smaller amplitude of the variation. In Fig.16, we show the ratios involving strangeness along the freeze-out lines, $T^2\chi_{BSS}/\chi_{BB}$, $m_2(S)$ and $T^2\chi_{BBSS}/\chi_{BB}$. As the critical region for strangeness is very small, these ratios are not sensitive to the singularity of the strange quark susceptibilities.

Finally, we show how m_1 and m_2 vary in relation to each other along the freeze-out line.[1] In Fig. 17, decreasing $\sqrt{s_{NN}}$ (increasing μ_B or decreasing T) starts from $m_1 = 0$ and continues in an anti-clockwise trajectory around the loop. The convergence of the lines at high T (close to $m_1 = 0$) is due to the convergence of the hypothetical freeze-out lines in our modeling, see Fig. 14 (top). For the lower T freeze-out lines (green dashed and blue dotted lines), the loop does not close. Even so, the low T/high μ end of the trajectory is the same for all freeze-out lines because the statistics and fluctuations are given by m, μ-dominated thermal distributions there. These plots show clearly the ordering of features

$$T_{\min,m_2} > T_{\max,m_1} > T_{\max,m_2} > T_{\rm CEP} \qquad (18)$$

which was found also in the GN and Ising models. (In the Ising model, we plot the kurtosis of the magnetization $\partial^4 M/\partial H^4$ versus the skewness $\partial^3 M/\partial H^3$ along lines of constant H, yielding a plot of the same shape as Fig. 17.) Again, the magnitudes of the m_1, m_2 are much greater for

[1] We thank R. Gavai for suggesting this plot.

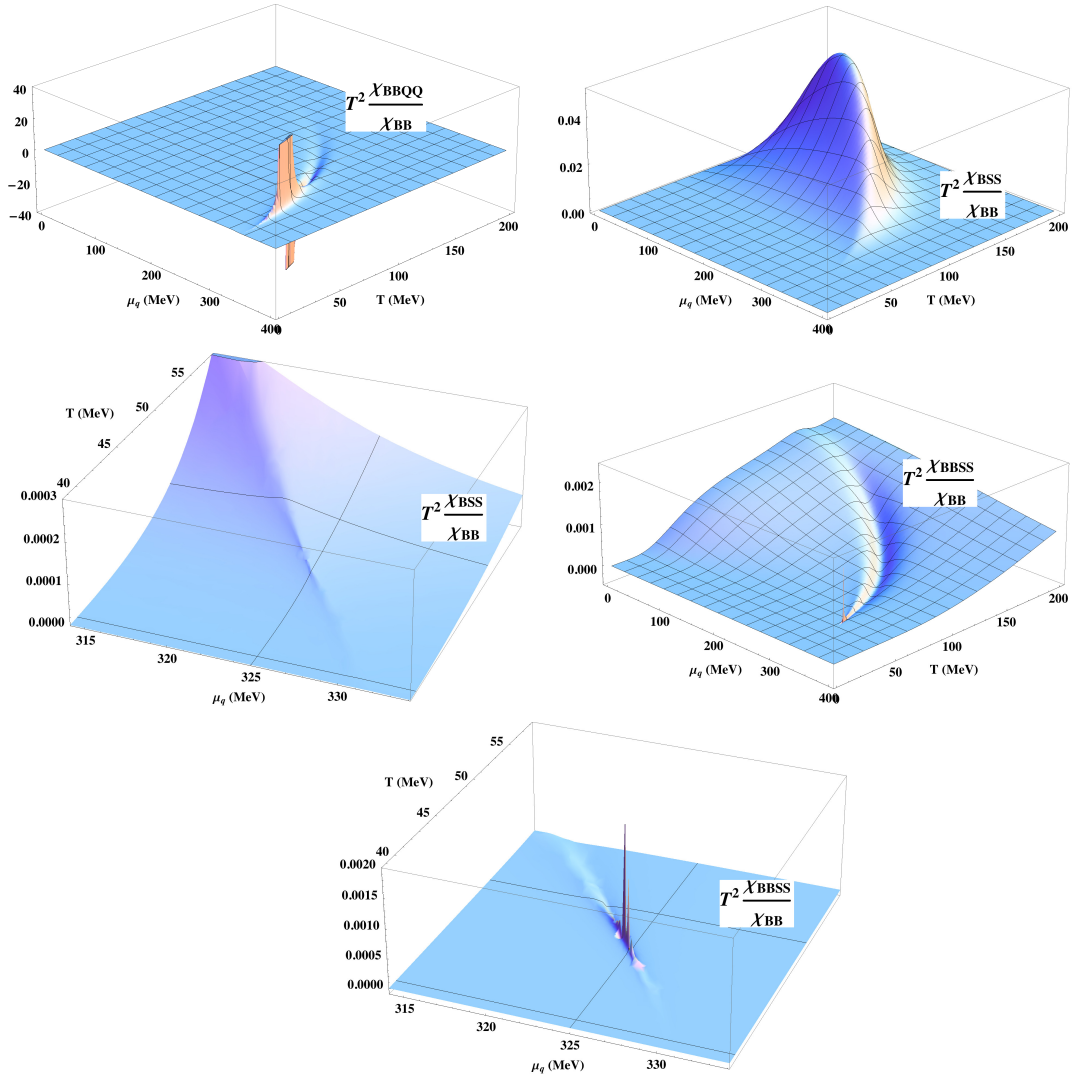

FIG. 11. m_1 and m_2 defined for non-vanishing cross-correlations in flavor. The vertical scale shows the singularities and variations in magnitude here are much smaller than in flavor-diagonal m_1, m_2 shown in Figs. 9 and 10. Only χ_{BBQQ}/χ_{BB} is comparable in magnitude, but according to Eq. (16) the singularity is dominated by the fourth-order quark susceptibility. Consequently, $\chi_{BBQQ} \simeq (1/4)\chi_B^{(4)}$ and the new information in the difference between these function is likely below experimental sensitivity.

baryon fluctuations than for charge fluctuations. We expect these characteristics are robust. Nonequilibrium effects and higher-order, model-dependent corrections will perturb the loop. However, given also the similarity to the GN and Ising results, it appears large corrections would be necessary to affect the ordering in Eq. (18). For ratios with strangeness, this ordering is not seen, because the critical region for strangeness is too small to impact the observables along the chosen freeze-out lines.

V. CONCLUSION

In this paper, we have investigated the behaviour of non-Gaussian fluctuations of baryon number, electric charge and strangeness on the phase diagram. Our purpose was to characterize their dependence at $\mu \neq 0$ and find robust qualitative features that can be used to help interpret experimental data in the search for a QCD critical point. To this end, we evaluated the third- and fourth-order susceptibilities in the NJL model, which is in the same universality class as QCD. Our analysis is limited to the mean-field approximation which means that we have not included several known corrections: modifications to the critical exponents controlling the divergence of the correlation length at the CEP, and model-dependent corrections described by higher-dimensional operators in the low energy effective field theory. The corrections to the critical exponents are better known quantitatively, but model-dependent corrections are less well-

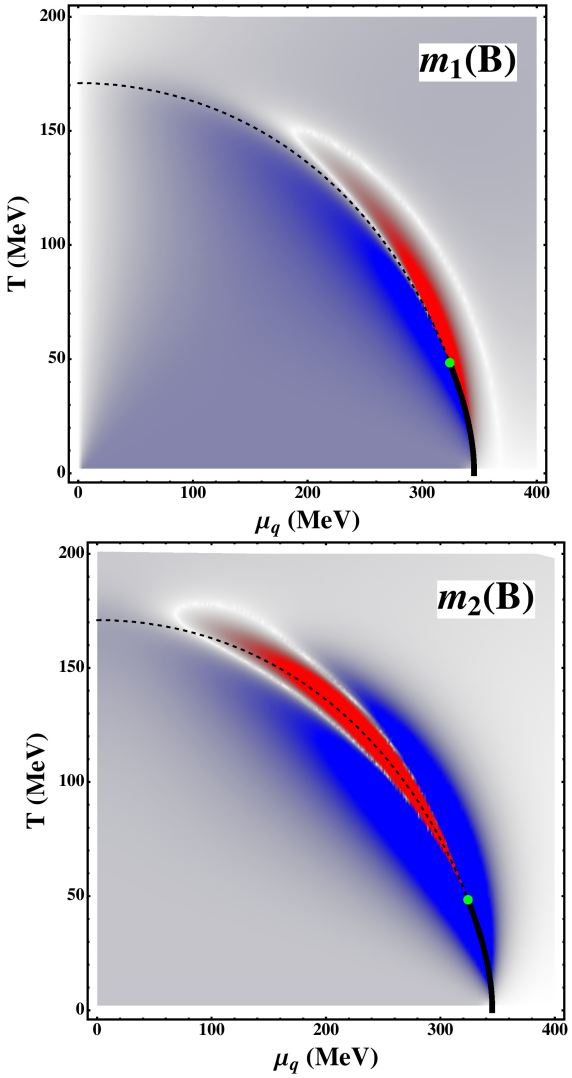

FIG. 12. For baryon susceptibility, the figures show the sign change of m_1 and m_2 on the phase diagram. Red areas are negative, and blue are positive. The green point indicates the location of CEP. The dashed thin line and the solid thick line stand for the crossover line and the first order phase transition line respectively.

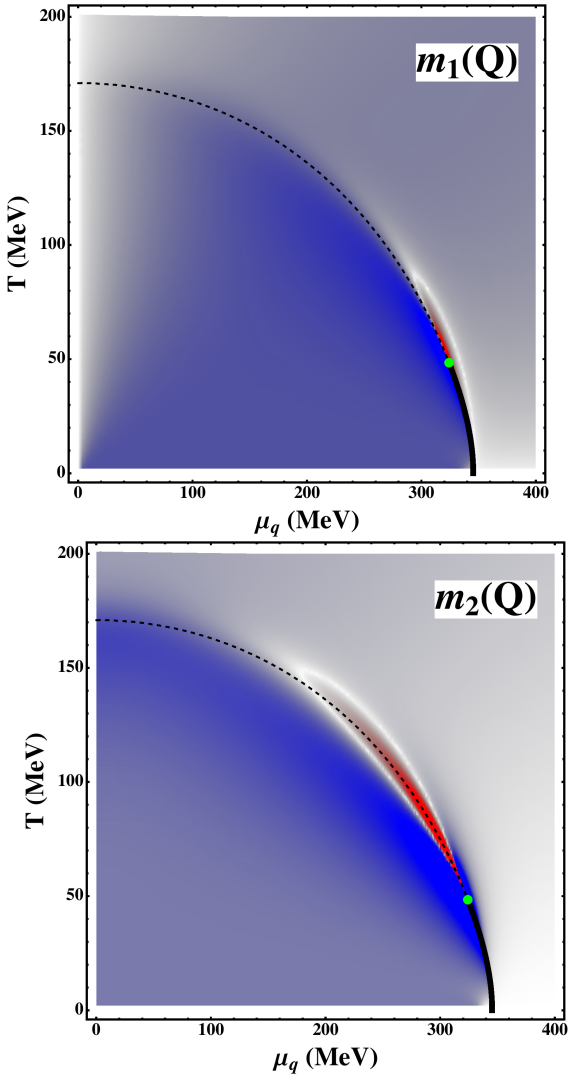

FIG. 13. m_1 and m_2 for charge, with colored regions to show sign changes. The area of the negative regions is smaller, as expected from the relative coefficient 1/4 for the most singular contributions.

controlled and their importance is not known in the context of the physical fireball where the correlation length of the critical mode may not be much larger than thermal correlation length.

We have given the quantitative results for all second-, third- and fourth-order susceptibilities. These plots show the accuracy of our diagrammatic approach in predicting the relevance of singular contributions in the context of multiple flavors. From this study, we see that the light quark susceptibilities remain everywhere the dominant singular contribution at the critical point. This result occurs despite both the isospin and strange-quark susceptibilities being also singular; both are numerically much smaller in magnitude than the light-quark susceptibilities. This also explains why charge fluctuations contain the same information as baryon fluctuations at leading order.

Having validated model-independent predictions from the diagrammatic analysis, we can identify several characteristics of the third- and fourth-order susceptibilities that are likely to be robust. These are:

1. Baryon number fluctuations are the largest in amplitude. This is because they are dominantly composed of the leading singular contributions from the light quark susceptibilities. Charge fluctuations are suppressed by numerical coefficients, as seen by comparing the expansions in Eq. (15) and Eq. (16). Strangeness fluctuations are the smallest in amplitude, though at high order they also show a singularity at the critical point. The strangeness fluctuations are suppressed by the relatively large

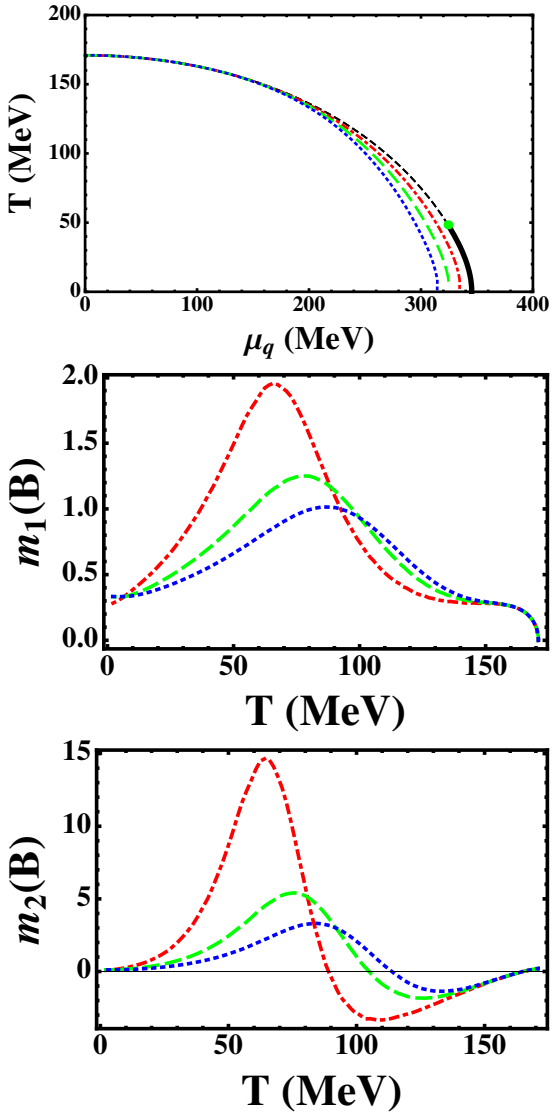

FIG. 14. Top frame: Hypothetical chemical freeze-out lines on the phase diagram to model the behaviour of the fluctuation ratios as a function of $\sqrt{s_{NN}}$. Middle and bottom frames: m_1 and m_2 of baryon number susceptibilities along these freeze-out lines, identified with lines in the top frame by color and dashing.

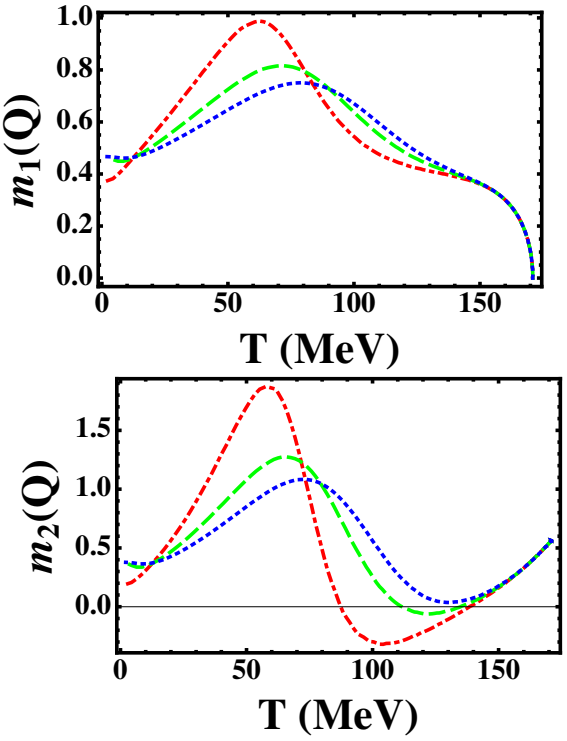

FIG. 15. Electrical charge m_1 and m_2 along the freeze-out lines defined in the top frame of Figure 14. The overall magnitude of variation is smaller than for $m_1(B), m_2(B)$.

bare mass of the strange quark, $m_s \sim T$.

2. The "critical region" where we see non-monotonicity in m_1 and m_2 along hypothetical freeze-out linesis largest for baryon number fluctuations. Therefore it provides the largest signal for freeze-outs occurring farther in the μ, T plane from the CP. This act follows from the amplitude of the fluctuations being largest.

3. The qualitative profile of the third and fourth order susceptibilities along the freeze-out line is model-independent. m_1 for both B, Q has a single peak at a temperature greater than the CP. m_2 has first a minimum and then a peak as the critical point is approached from high T (equivalently larger collision energy $\sqrt{s_{NN}}$). The $m_2 < 0$ negative region may be accessible at chemical freeze-out in the symmetry broken phase. These behaviours have been seen in the GN and NJL models.

4. The features of the m_1 and m_2 freeze-out profiles obey a numerical ordering temperature or collision energy, given by Eq. (18). This is demonstrated by plotting m_2 versus m_1 along the freeze-out line, and we have argued this trajectory is difficult to change in qualitative features.

It is our hope that these features can aid the interpretation of experimental data for the third- and fourth-order susceptibilities. Although our results may support preliminary indications of critical behaviour in the data, it is clear that much more work is required to identify these signatures with a QCD critical point.

Appendix A: NJL model

In our study, we consider the 3-flavor NJL model with two degenerate light quarks and a heavier strange quark.

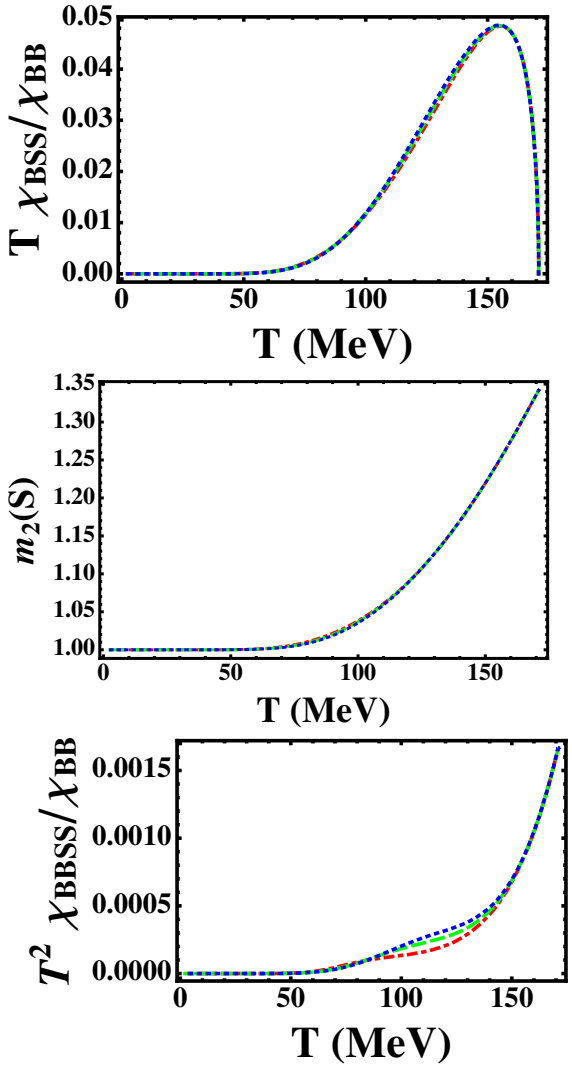

FIG. 16. The strangeness-dependent ratios $T\chi_{BSS}/\chi_{BB}$, $m_2(S)$ and $T^2\chi_{BBSS}/\chi_{BB}$ along the chemical freeze-out lines defined in the top frame of Figure 14. The small magnitude of the singularity in these observables means they do not significantly impact even the freeze-out line passing nearest to the CEP.

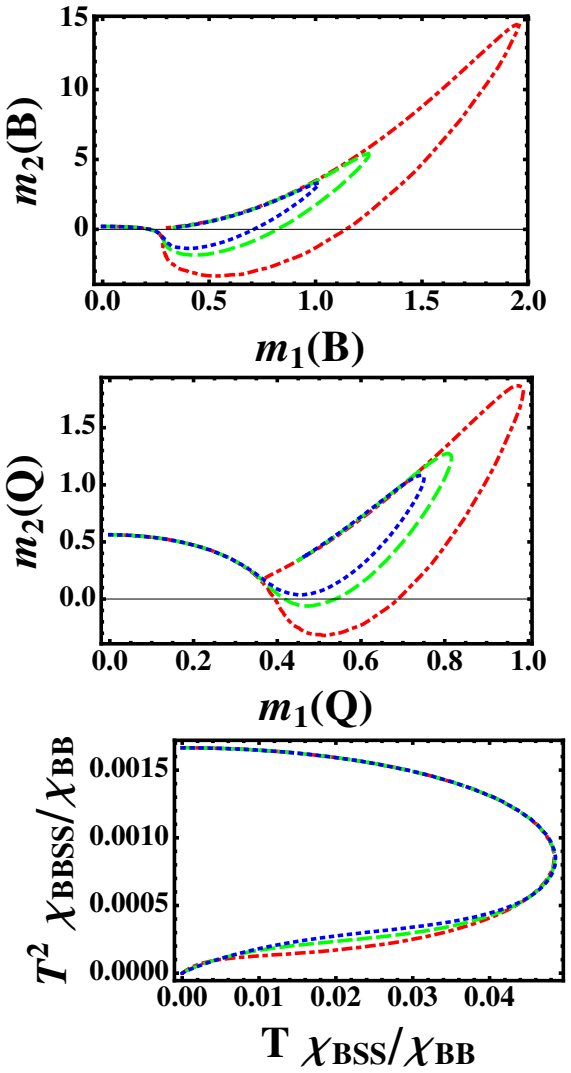

FIG. 17. Top: $m_2(B)$ versus $m_1(B)$ along the freeze-out line. Temperature decreases following the loop anti-clockwise, exhibiting the temperature ordering Eq. (18). Middle: $m_2(Q)$ versus $m_1(Q)$ along the freeze-out line, displaying the same features as the top plot for baryon fluctuations, but with smaller magnitude fluctuations for charge. Bottom: an analogous plot for strangeness-fluctuation observables. Although χ_{BBSS} and χ_{BSS} both exhibit criticality, our chosen freeze-out lines do not pass near enough to show the impact of the divergence near the critical point.

The quark level Lagrangian is

$$\mathcal{L} = \sum_{i=u,d,s} \bar{\psi}_i(\partial\!\!\!/ - m_i)\psi_i + G\mathrm{Tr}[(\bar{\psi}\lambda_a\psi)^2 + (\bar{\psi}\gamma_5\lambda_a\psi)^2] - K(\det\bar{q}(1-\gamma_5)q + \det\bar{q}(1+\gamma_5)q) \quad \text{(A1)}$$

The model parameters are the "bare" quark masses m_i and the 4-fermion couplings G, K. In addition, for numerical evaluation of the effective potential below we must introduce a momentum cutoff Λ. These five model parameters (Λ, m_u, m_s, G, K) are fixed by matching the four physical quantities pion, kaon, η' masses and the pion decay constant in vacuum, $m_\pi = 138\,\mathrm{MeV}$, $m_K = 495\,\mathrm{MeV}$, $m_{\eta'} = 958\,\mathrm{MeV}$ and $f_\pi = 93\,\mathrm{MeV}$. Being the arbitrary renormalization scale, Λ is not completely fixed, and one can choose to work at different Λs.

We have used the following parameter set[23, 36, 37]

$$m_u = m_d = 5\,\mathrm{MeV}, \quad m_s = 136\,\mathrm{MeV}, \quad \text{(A2)}$$

$$\Lambda = 631\,\mathrm{MeV}, \quad G\Lambda^2 = 1.83, \quad K\Lambda^5 = 9.29 \quad \text{(A3)}$$

Spontaneous symmetry breaking leading to nonzero light quark condensates $\langle\bar{u}u\rangle, \langle\bar{d}d\rangle \neq 0$ has greater impact on phenomenology than the explicit breaking from their masses, as is the case in QCD.

Although physical observables have been used to fix the model parameters, the calculated physical observables may exhibit residual cutoff dependence. Parame-

ter dependence in the NJL model has been studied in Ref. [37]. Being an effective theory, the NJL lagrangian contains an infinite tower of higher dimensional non-renormalizable interactions. We have truncated the Lagrangian to include only two non-renormalizable interactions. Therefore, even though the parameters of the Lagrangian are fixed by fitting to physical observables, predictions of other physical observables can contain residual cutoff dependence.

To solve the model and study the phase diagram, we take the mean field approximation. After shifting the quark bilinears with their vacuum expectation values $\bar{q}q \to \langle\bar{q}q\rangle + \varphi_q$, the quark fields can be integrated out, and we obtain an effective potential depending only on T, μ_q and φ_q ($q = u, d, s$). As long as the isospin chemical potential

$$\mu_I = \mu_u - \mu_d \lesssim \frac{m_\pi}{2} \simeq 65 \text{ MeV} \tag{A4}$$

the u, d condensates are equal and transition at the same μ, T. Pseudoscalar, vector and pseudovector diquark condensates are also suppressed and can be ignored. Experimental data indicates that this condition holds even at the lowest collision energies. The resulting effective potential has the form

$$\Omega = 2G(\sigma_u^2 + \sigma_d^2 + \sigma_s^2) - 4K\sigma_u\sigma_d\sigma_s + \sum_{f=u,d,s} \Omega_f \tag{A5}$$

$$\Omega_f = -2N_c \int \frac{d^3p}{(2\pi)^3} \Big(E_f \Theta(\Lambda^2 - p^2) + T\ln(1 + e^{-\beta(E_f - \mu_f)}) + T\ln(1 + e^{-\beta(E_f + \mu_f)}) \Big) \tag{A6}$$

where $\Theta(x)$ is the Heaviside step function, $E_f^2 = \vec{p}^2 + M_f^2$. The last two terms in Ω_f are respectively the particle and antiparticle fermi distributions including the chemical potential. The M_f are effective masses, functions of the condensates

$$M_f = m_f - 4G\sigma_f + 2K\sigma_{f'}\sigma_{f''}, \quad (f \neq f' \neq f'') \tag{A7}$$

The term off-diagonal in flavor implies that the strange quark condensate is discontinuous where the light quark condensates are discontinuous and vice versa. The larger bare mass of the strange quark means the impact of explicit chiral symmetry breaking is larger than for the light quarks, and its phase transition occurs only for larger chemical potential and temperature, see [29] for discussion how the position of the critical point depends on the bare quark mass. If a critical point is accessible to lattice or HIC, it will be the light quark critical line, which is at lower chemical potential and temperature. However, due to the flavor coupling, some evidence of the criticality will be manifest in the strange susceptibilities. We will discuss this point further below.

The phase diagram is determined by solving the coupled set of gap equations

$$0 = \frac{\partial\Omega}{\partial\sigma_\alpha} = \sum_\gamma \left(4G\delta_{\alpha\gamma} - 2K \sum_\theta |\epsilon_{\alpha\gamma\theta}|\sigma_\theta \right) \Delta_\gamma \tag{A8}$$

$$\Delta_\gamma = \sigma_\gamma - \frac{\partial\Omega_\gamma}{\partial m_\gamma}$$

taking the solution that corresponds to the global minimum of the effective potential. ($|\epsilon_{\alpha\gamma\theta}|$ tensor is $+1$ in entries with $\alpha \neq \gamma \neq \theta$.) We solve the system using two independent numerical methods, as a quantitative check on our results.

Appendix B: Diagrammatic system

μ-derivatives of the pressure include a term for each flavor

$$\frac{dP(T, \vec{\mu}, \vec{\sigma})}{d\mu_\alpha} = \frac{\partial P}{\partial \mu_\alpha} + \sum_\beta \left.\frac{\partial P}{\partial \sigma_\beta}\right|_{\vec{\sigma}^{(0)}} \frac{\partial \sigma_\beta}{\partial \mu_\alpha} \tag{B1}$$

The vectors $\vec{\mu}, \vec{\sigma}$ are shorthand for $(\mu_u, \mu_d, \mu_s), (\sigma_u, \sigma_d, \sigma_s)$, and $\vec{\sigma}^{(0)}$ subscript indicates the derivative is evaluated at the minimum of the potential. The last factor $\partial\sigma_\beta/\partial\mu_\alpha$ can be rewritten using the fact that the gap equation is independent of the chemical potential

$$\begin{aligned} 0 &= \frac{d}{d\mu_\alpha} \left(\left.\frac{\partial P}{\partial \sigma_\beta}\right|_{\vec{\sigma}^{(0)}} \right) \\ &= \left.\frac{\partial^2 P}{\partial\mu_\alpha \partial\sigma_\beta}\right|_{\vec{\sigma}^{(0)}} + \sum_\gamma \left.\frac{\partial^2 P}{\partial\sigma_\beta \partial\sigma_\gamma}\right|_{\vec{\sigma}^{(0)}} \frac{\partial\sigma_\gamma}{\partial\mu_\alpha} \end{aligned} \tag{B2}$$

Note that the second term contains a factor which has the form of a two-point correlator of the σ field.

When we write out a general (second order) susceptibility, we find two terms

$$\begin{aligned} \chi_{\alpha\beta} &= \frac{d^2 P}{d\mu_i d\mu_j} \\ &= \frac{\partial^2 P}{\partial\mu_\alpha\partial\mu_\beta} - \sum_{\gamma,\delta} \frac{\partial^2 P}{\partial\mu_\alpha\partial\sigma_\gamma} \left(\left.\frac{\partial^2 P}{\partial\sigma_\gamma\partial\sigma_\delta}\right|_{\vec{\sigma}^{(0)}} \right)^{-1} \frac{\partial^2 P}{\partial\sigma_\delta\partial\mu_\beta} \end{aligned} \tag{B3}$$

A similar relation has been discussed by [38, 39]. The first is the second derivative at the minimum of the potential, and the second relates μ-derivatives at different points through the σ two-point function. We express this naturally by the diagrams in Figure 1. This "σ correlator"

$$\frac{\partial^2\Omega}{\partial\sigma_\alpha\partial\sigma_\beta} = \sum_\gamma \left(4G\delta_{\alpha\gamma} - 2K \sum_\theta |\epsilon_{\alpha\gamma\theta}|\sigma_\theta \right) \frac{\partial\Delta_\gamma}{\partial\sigma_\beta} \tag{B4}$$

$$\frac{\partial\Delta_\gamma}{\partial\sigma_\beta} = \delta_{\gamma\beta} - \frac{\partial^2\Omega_\gamma}{\partial m_\gamma^2} \left(4G\delta_{\beta\gamma} - 2K \sum_\theta |\epsilon_{\beta\gamma\theta}|\sigma_\theta \right)$$

is not diagonal in flavor space due to the anomaly-induced interaction (proportional to K).

The third and fourth order susceptibilities include new terms, such as the σ three- and four-point functions. By writing out all the diagrams constructed from these pieces, one may search higher order susceptibilities for their most singular contributions.

Acknowledgments: We would like to thank R. Gavai and C. Markert for suggestions and discussions. J.D. is supported in part by the Major State Basic Research Development Program in China (Contract No. 2014CB845406), National Natural Science Foundation of China (Projects No. 11105082). J.W.C. is supported in part by the MOST, NTU-CTS, NTU-CASTS of R.O.C., and the DFG and NSFC (CRC 110). H.K. is supported by Ministry of Science and Technology (Taiwan, ROC), through Grant No. MOST 103-2811-M-002-087. L.L. is supported by NNSA cooperative agreement de-na0002008, the Defense Advanced Research Projects Agencys PULSE program (12-63-PULSE-FP014), the Air Force Office of Scientific Research (FA9550-14-1-0045) and the National Institute of Health SBIR 1 LPT_001.

[1] M. A. Stephanov, PoS LAT **2006**, 024 (2006) [hep-lat/0701002]; K. Fukushima and C. Sasaki, Prog. Part. Nucl. Phys. **72**, 99 (2013) [arXiv:1301.6377 [hep-ph]].
[2] S. Gupta, X. Luo, B. Mohanty, H. G. Ritter and N. Xu, Science **332**, 1525 (2011) [arXiv:1105.3934 [hep-ph]]; and references therein.
[3] M. M. Aggarwal *et al.* [STAR Collaboration], Phys. Rev. Lett. **105**, 022302 (2010) [arXiv:1004.4959 [nucl-ex]].
[4] L. Adamczyk *et al.* [STAR Collaboration], Phys. Rev. Lett. **112**, 032302 (2014) [arXiv:1309.5681 [nucl-ex]].
[5] Z. Fodor and S. D. Katz, Phys. Lett. B **534**, 87 (2002) [hep-lat/0104001].
[6] C. R. Allton, S. Ejiri, S. J. Hands, O. Kaczmarek, F. Karsch, E. Laermann, C. Schmidt and L. Scorzato, Phys. Rev. D **66**, 074507 (2002) [hep-lat/0204010].
[7] P. de Forcrand and O. Philipsen, Phys. Rev. Lett. **105**, 152001 (2010) [arXiv:1004.3144 [hep-lat]];
[8] R. V. Gavai and S. Gupta, Phys. Lett. B **696**, 459 (2011) [arXiv:1001.3796 [hep-lat]].
[9] A. Li, A. Alexandru and K. F. Liu, Phys. Rev. D **84**, 071503 (2011) [arXiv:1103.3045 [hep-ph]].
[10] G. Endrodi, Z. Fodor, S. D. Katz and K. K. Szabo, JHEP **1104**, 001 (2011) [arXiv:1102.1356 [hep-lat]].
[11] C. Schmidt [BNL-Bielefeld-CCNU Collaboration], PoS LATTICE **2014**, 186 (2015).
[12] M. A. Stephanov, K. Rajagopal and E. V. Shuryak, Phys. Rev. Lett. **81**, 4816 (1998) [hep-ph/9806219]. M. A. Stephanov, K. Rajagopal and E. V. Shuryak, Phys. Rev. D **60**, 114028 (1999) [hep-ph/9903292].
[13] M. A. Stephanov, Phys. Rev. Lett. **102**, 032301 (2009) [arXiv:0809.3450 [hep-ph]].
[14] M. Asakawa, S. Ejiri and M. Kitazawa, Phys. Rev. Lett. **103**, 262301 (2009) [arXiv:0904.2089 [nucl-th]].
[15] M. A. Stephanov, Phys. Rev. Lett. **107**, 052301 (2011) [arXiv:1104.1627 [hep-ph]].
[16] B. Berdnikov and K. Rajagopal, Phys. Rev. D **61**, 105017 (2000) [hep-ph/9912274]. C. Nonaka and M. Asakawa, Phys. Rev. C **71**, 044904 (2005) [nucl-th/0410078]. C. Athanasiou, K. Rajagopal and M. Stephanov, Phys. Rev. D **82**, 074008 (2010) [arXiv:1006.4636 [hep-ph]].
[17] V. Koch, arXiv:0810.2520 [nucl-th].
[18] Y. Nambu and G. Jona-Lasinio, Phys. Rev. **122**, 345 (1961); **124**, 246 (1961).
[19] V. Bernard, R. L. Jaffe and U. G. Meissner, Phys. Lett. B **198**, 92 (1987).
[20] V. Bernard, R. L. Jaffe and U. G. Meissner, Nucl. Phys. B **308**, 753 (1988).
[21] U. Vogl and W. Weise, Prog. Part. Nucl. Phys. **27**, 195 (1991).
[22] S. P. Klevansky, Rev. Mod. Phys. **64**, 649 (1992).
[23] T. Hatsuda and T. Kunihiro, Phys. Rept. **247**, 221 (1994).
[24] M. Buballa, Phys. Rept. **407**, 205 (2005).
[25] M. Huang, Int. J. Mod. Phys. E **14**, 675 (2005).
[26] V. Skokov, B. Friman and K. Redlich, Phys. Lett. B **708**, 179 (2012) [arXiv:1108.3231 [hep-ph]].
[27] W. j. Fu and Y. l. Wu, Phys. Rev. D **82**, 074013 (2010) [arXiv:1008.3684 [hep-ph]].
[28] X. y. Xin, S. x. Qin and Y. x. Liu, Phys. Rev. D **90**, no. 7, 076006 (2014).
[29] J. W. Chen, J. Deng and L. Labun, Phys. Rev. D **92**, 054019 (2015) [arXiv:1410.5454 [hep-ph]].
[30] S. Das [STAR Collaboration], EPJ Web Conf. **90**, 10003 (2015) [arXiv:1412.0350 [nucl-ex]].
[31] M. Petrán, J. Letessier, V. Petráček and J. Rafelski, Phys. Rev. C **88**, no. 3, 034907 (2013) [arXiv:1303.2098 [hep-ph]].
[32] J. Cleymans, B. Kampfer, M. Kaneta, S. Wheaton and N. Xu, Phys. Rev. C **71**, 054901 (2005) [hep-ph/0409071].
[33] T. Xia, L. He and P. Zhuang, Phys. Rev. D **88**, no. 5, 056013 (2013) [arXiv:1307.4622].
[34] Y. Hatta and M. A. Stephanov, Phys. Rev. Lett. **91**, 102003 (2003) [Erratum-ibid. **91**, 129901 (2003)] [hep-ph/0302002].
[35] P. Costa, C. A. de Sousa, M. C. Ruivo and Y. L. Kalinovsky, Phys. Lett. B **647**, 431 (2007) doi:10.1016/j.physletb.2007.02.045 [hep-ph/0701135].
[36] K. Kashiwa, H. Kouno, M. Matsuzaki and M. Yahiro, Phys. Lett. B **662**, 26 (2008) doi:10.1016/j.physletb.2008.01.075 [arXiv:0710.2180 [hep-ph]].
[37] K. Fukushima, Phys. Rev. D **77**, 114028 (2008).
[38] H. Fujii, Phys. Rev. D **67**, 094018 (2003) [hep-ph/0302167].
[39] S. K. Ghosh, A. Lahiri, S. Majumder, M. G. Mustafa, S. Raha and R. Ray, Phys. Rev. D **90**, no. 5, 054030 (2014) [arXiv:1407.7203 [hep-ph]].